Research Article

Ravi Anant Kishore, Anthony Marin, and Shashank Priya*

Efficient Direct-Drive Small-Scale Low-Speed Wind Turbine

Abstract: There is growing need for the green, reliable, and cost-effective power solution for the expanding wireless microelectronic devices. In many scenarios, these needs can be met through a small-scale wind energy portable turbine (SWEPT) that operates near ground level where wind speed is of the order of few meters per second. SWEPT is a three-bladed, 40 cm rotor diameter, direct-drive, horizontal-axis wind turbine that has very low cut-in wind speed of 1.7 m/s. It operates in a wide range of wind speeds between 1.7 m/s and 10 m/s and produces rated power output of 1 W at wind speed of 4.0 m/s. The wind turbine is capable of producing electrical power up to 9.8 W at wind speed of 10 m/s. The maximum efficiency of SWEPT was found to be around 21% which makes it one of the most efficient wind turbines reported at the small scale and low wind speed. These advancements open many new opportunities for embedding and utilizing wireless and portable devices.

Keywords: small-scale wind turbine, wind tunnel, power coefficient, wind energy, portable power

*Corresponding author: Shashank Priya, Department of Mechanical Engineering, Center for Energy Harvesting Materials and Systems (CEHMS), Bio-Inspired Materials and Devices Laboratory (BMDL), Virginia Tech, 310 Durham Hall, Blacksburg, VA 24061, USA, E-mail: spriya@vt.edu
Ravi Anant Kishore: E-mail: ravi86@vt.edu, Anthony Marin: E-mail: marinvt@gmail.com, Department of Mechanical Engineering, Center for Energy Harvesting Materials and Systems (CEHMS), Bio-Inspired Materials and Devices Laboratory (BMDL), Virginia Tech, 310 Durham Hall, Blacksburg, VA 24061, USA
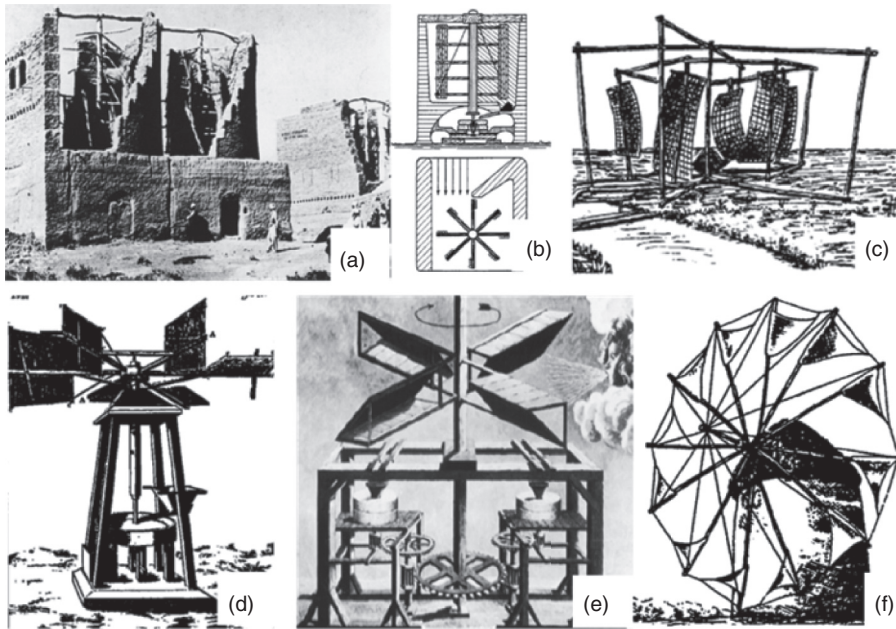
Introduction

Historical development of wind turbines

Wind energy is one of the most abundant renewable energy resources and it has been targeted for centuries. It is predicted that human beings have been using wind energy in their daily work for about 4,000 years (http://www.wwindea.org/technology/ch01/estructura-en.htm). As early as 1700 BC, King Hammurabi of Babylon used wind powered scoops to irrigate the plains of Mesopotamia (Gasch and Twele 2012). Wind was also used to grind grain and that is the reason why we still speak of "windmills", even though they are now hardly used for grinding grains (http://www.wwindea.org/technology/ch01/estructura-en.htm). Figure 1 displays some of the primitive windmills used by early human civilizations (Gasch and Twele 2012).

It can be noted that most of the world's oldest windmills had vertical axis of rotation. Initial designs (Figure 1 (a)–(c)) were very simple, especially from construction point of view. Braided mats or sails were utilized to generate drag and thus to rotate the windmills about the central axis. The vertical-axis windmills had another operational advantage that they were independent of wind direction. Figure 1(d) and (e) shows some later versions of vertical-axis mills developed in France and Italy, respectively. In Figure 1(d), the millstone is attached directly to the vertical drive shaft without any intermediate gear or other mechanism to redirect the rotational movement. Figure 1(e) shows one of the advanced windmills created by Fausto Veranzio in Italy (Gasch and Twele 2012). It can be seen that this windmill is engineered with cup-shaped rotor blades which improves the efficiency of the device. Veranzio also developed a gearing mechanism for his windmills which allows millstones to run at much higher speed, even though the rotors were designed for low tip speed ratio (Gasch and Twele 2012).

The horizontal-axis windmills are a relatively newer invention than the vertical-axis windmills. Though the first documentation of the horizontal-axis windmills dates back to the twelfth century, the theoretical descriptions regarding the driving power of horizontal-axis devices, i.e. lift forces on the blades, was investigated only during the beginning of the twentieth century (Gasch and Twele 2012). One of the most popular early horizontal-axis wind turbines (HAWTs) was the tower

Figure 1　Some of the world's oldest windmills; (a) Ruins of a vertical-axis windmill in Afghanistan, approx. 700 AD (picture taken in 1977); (b) Persian windmill; (c) Chinese windmill with flapping sails, approx. 1000 AD; (d) Vertical-axis windmills with flapping sails, France 1719 AD; (e) Vertical-axis windmills with bodies driven by drag forces, Italy, approx. 1600 AD; and (f) Mediterranean tower mill with sails. All pictures are adapted from Gasch and Twele (2012)

mills, shown in Figure 1(f), which existed in southern Europe. The first written evidence of such windmills dates back to the thirteenth century (Gasch and Twele 2012). There were some other types of horizontal-axis windmills which existed in different parts of the world (mainly in the Occident) during different periods of time: *Post windmill* (1100s), *Wipmolen Dutch* (1400s), *Dutch smock mill* (1500s), *Paltrock mill* (1600s), and *Gallery smock mill* (1700s). Brief description about these windmills can be found in Gasch and Twele (2012). However,

none of the historical HAWTs gained as much popularity as the American farm windmill (sometimes also called Western mill). These windmills were developed in the mid-nineteenth century mainly to provide drinking water to people and cattle in North America. Moreover, they were used to assure the water supply for the steam locomotives of the new railways expanding into the West (Gasch and Twele 2012). Figure 2(a) shows an early advertisement for the American windmills by U.S. Wind Engine & Pumping Co., the company who developed this

Figure 2　American windmills (Western windmills): (a) an advertisement by U.S. Wind Engine & Pumping Co., developer of the American windmills (http://www.ironmanwindmill.com/windmill-history.htm), and (b) a wind farm utilizing the American windmills for water pumping (http://www.midamericawindmillmuseum.org/imgs/home/windmill_2.jpg)

windmill (http://www.ironmanwindmill.com/windmill-history.htm). The most important component of this windmill is the rotor, which is also called "rotor rosette" because of its structural design. Its diameter varies between 3 m and 5 m and has more than 20 metal sheet blades. It also consists of a tail that allows the rotor to turn automatically so that it always faces the incident wind. It uses a crank shaft to drive a piston pump. The American mills are still in existence, and several of them are installed with a nearly unchanged design in Australia, Argentina, and the USA (http://www.ironman-windmill.com/windmill-history.htm). Figure 2(b) depicts one of such wind farms utilizing the American mills for water pumping (http://www.midamericawindmillmuseum.org/imgs/home/windmill_2.jpg).
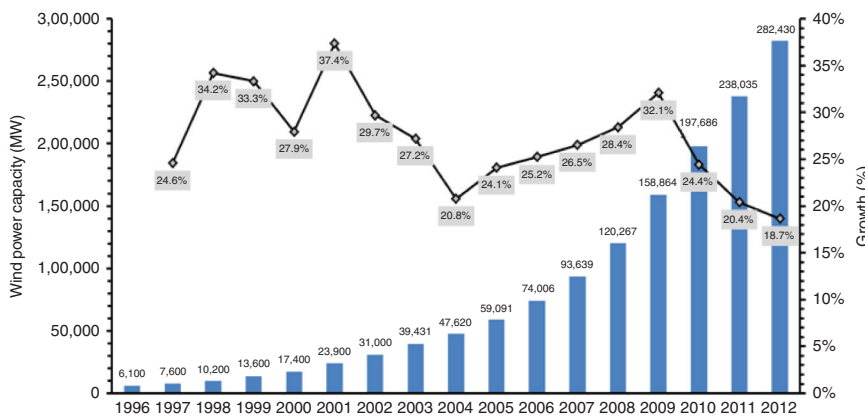
Current status of wind energy

The fourth edition of the Global Wind Energy Outlook released on November 14, 2012 at Beijing by Greenpeace International and the Global Wind Energy Council states that wind power currently provides about 3.5% of global electricity demand, and it is expected that the wind energy share could reach up to 12% by 2020 (http://www.gwec.net/publications/global-wind-energy-outlook/global-wind-energy-outlook-2012/). Figure 3 shows the global cumulative installed wind power capacity over last 17 years (Global Wind Energy Council Report 2012). At the end of year 2012, the world-wide total wind power capacity was 282 GW, showing a growth of about 18.7% (44 GW) over the preceding year. It is important to note that although the year 2012 created a new record in total installed wind power capacity, the wind market has cooled down in relative terms. If we look at the annual

growth rate, it had continued to increase since the year 2004, peaking at 32.1% in year 2009. However, since then the growth has decreased substantially. In 2012, the global growth went down to 18.7%, which is the lowest rate in the last two decades, according to a report by the World Wind Energy Association (Gsänger and Pitteloud 2012).

Table 1 presents cumulative wind power capacity from year 2008 to 2012 in top 10 countries and the same variable worldwide (Global Wind Energy Council Report 2012; Gsänger and Pitteloud 2012). The data indicate that even though the global wind power capacity exhibited the low growth rate (18.7%) in year 2012, it increased over 133.5% during the last 5 years. It is also very interesting to note that 73.7% of the total power capacity (282,430 MW) in 2012 was contributed by five countries, i.e. China, USA, Germany, Spain, and India. China's wind power

Table 1 Cumulative wind power capacity outlook from 2008 to 2012 (Global Wind Energy Council Report 2012; Gsänger and Pitteloud 2012)

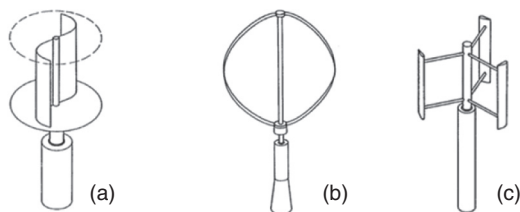| Country	1) Total capacity (MW)					Growth rate 2012 (%)
	2008	2009	2010	2011	2012	
China	12,210	25,810	44,733	62,364	75,564	21.2
USA	25,237	35,159	40,180	46,919	60,007	27.9
Germany	23,897	25,777	27,215	29,075	31,332	7.8
Spain	16,689	19,149	20,676	21,673	22,796	5.2
India	9,587	11,807	13,065	15,880	18,421	16.0
UK	3,195	4,092	5,203	6,018	8,445	40.3
Italy	3,736	4,850	5,797	6,737	8,144	20.9
France	3,404	4,574	5,660	6,640	7,196	8.4
Canada	2,369	3,319	4,008	5,265	6,200	17.8
Portugal	2,862	3,357	3,702	4,093	4,525	10.6
Worldwide	120,986	159,837	197,040	238,035	282,482	18.7

Figure 3 Total installed wind power capacity (MW) and world wind power market growth rate (%) 1996–2012. Information taken from Global Wind Energy Council Report (2012)

capacity continued to grow at the rate of over 21% in 2012. The United States has also gained the momentum and displayed the annual growth rate of 27.9% in 2012, which is the highest growth rate in last three consecutive years. The installed wind power capacity in USA has reached up to 60,007 MW by the end of year 2012. In 2012, the electricity produced from wind power in the United States totaled to about 140 TW h, which is around 3.5% of net electricity generation by all the energy sources (http://www.eia.gov/electricity/monthly/pdf/epm.pdf). The U.S. Department of Energy envisions supplying 20% of all U.S. electricity from wind power by 2030 (WIND AND WATER POWER PROGRAM 2011).

Classification of wind turbines

There are broadly three ways to classify the wind turbines: (i) on the basis of the orientation of axis of rotation (vertical or horizontal), (ii) on the basis of the component of aerodynamic forces (lift or drag) that powers the wind turbine, and (iii) on the basis of energy generating capacity (micro, small, medium, or large).

There are essentially two kinds of wind turbines, when they are categorized on the basis of their orientation of the axis of rotation: vertical-axis wind turbines (VAWTs) and Horizontal-axis wind turbines (HAWTs). As the name suggests, the rotor of VAWTs rotates perpendicular to the ground while that of HAWTs spins parallel to the ground. It was explained in the previous section that most of the early wind turbines were vertical axis, because they were relatively simple to construct (especially for the milling purpose) and they also did not require any mechanism to orient themselves in the direction of wind. In spite of these attributes, none of the old designs of VAWTs survived for long time. Currently, there are three most popular designs of VAWTs: (a) Savonius VAWT, (b) curved-blade Darrieus VAWT, and (c) straight-blade VAWT (Islam, Ting, and Fartaj 2008). Figure 4(a)–(c) shows Savonius, curved-blade Darrieus, and straight-blade Darrieus VAWT rotors,

Figure 4 VAWTs: (a) Savonius rotor, (b) curved-blade Darrieus rotor, and (c) straight-blade Darrieus rotor (http://www.elite.tugraz.at/Jungbauer/3.htm)

respectively (http://www.elite.tugraz.at/Jungbauer/3.htm). Savonius turbines are drag-type, because it utilizes drag component of the aerodynamic force to rotate, while Darrieus turbines are lift-type because it is the lift component of the aerodynamic force that powers the Darrieus rotor. In principle, Savonius rotors normally have two cups or half drums attached to a central shaft in opposing directions, as shown in Figure 4(a). The drum, which is against the wind flow, catches the wind and creates a moment along the axis. The aerodynamic torque by the first drum rotates the rotor and brings the opposing drum against the wind flow. The second drum now catches the wind and causes the rotor to rotate even further and thus completes a full rotation. This process continues until there is sufficient wind to turn the axial shaft which is normally connected to a pump or a generator (Islam, Ting, and Fartaj 2008). Savonius turbines generally have poor efficiency (less than 25%) and that is why they are not so commercially successful but there are some advantages such as simple construction with low cost, high static and dynamic moment, wind acceptance from any direction, low noise and angular velocity in operation, and reduced wear on moving parts which justifies their operation for low power applications (Akwa, Vielmo, and Petry 2012).

The Darrieus-type VAWTs consists of two or more blades which are attached to a vertical central shaft. These blades can be curved (as shown in Figure 4(b)) or they can be straight (as shown Figure 4(c)). Irrespective of the curvature, the blades always have airfoil profile that creates aerodynamic lift, when they are exposed to the incident wind. This phenomenon creates moment along the axis and causes the central shaft to rotate, which ultimately runs the generator to produce electricity. The curved-blade Darrieus VAWTs have lower bending stress in the blades as compared to straight-blade Darrieus VAWTs and therefore former is more commercially successful (Islam, Ting, and Fartaj 2008). However, on the small-scale power production, the straight-bladed Darrieus VAWTs are more popular because of their simple blade design (Akwa, Vielmo, and Petry 2012). The straight-bladed Darrieus VAWTs sometimes may have variable pitch angle. It has been found that constant pitch straight-bladed Darrieus VAWTs do not have self-start ability (Kirke 1998). The variable pitch configuration of the blades allows Darrieus VAWTs to overcome the starting torque problem but it is overly complicated, making them quite impractical for small-scale power generation (Islam, Ting, and Fartaj 2008).

At present, HAWTs are the most popular among all windmill designs. This is primarily because HAWTs
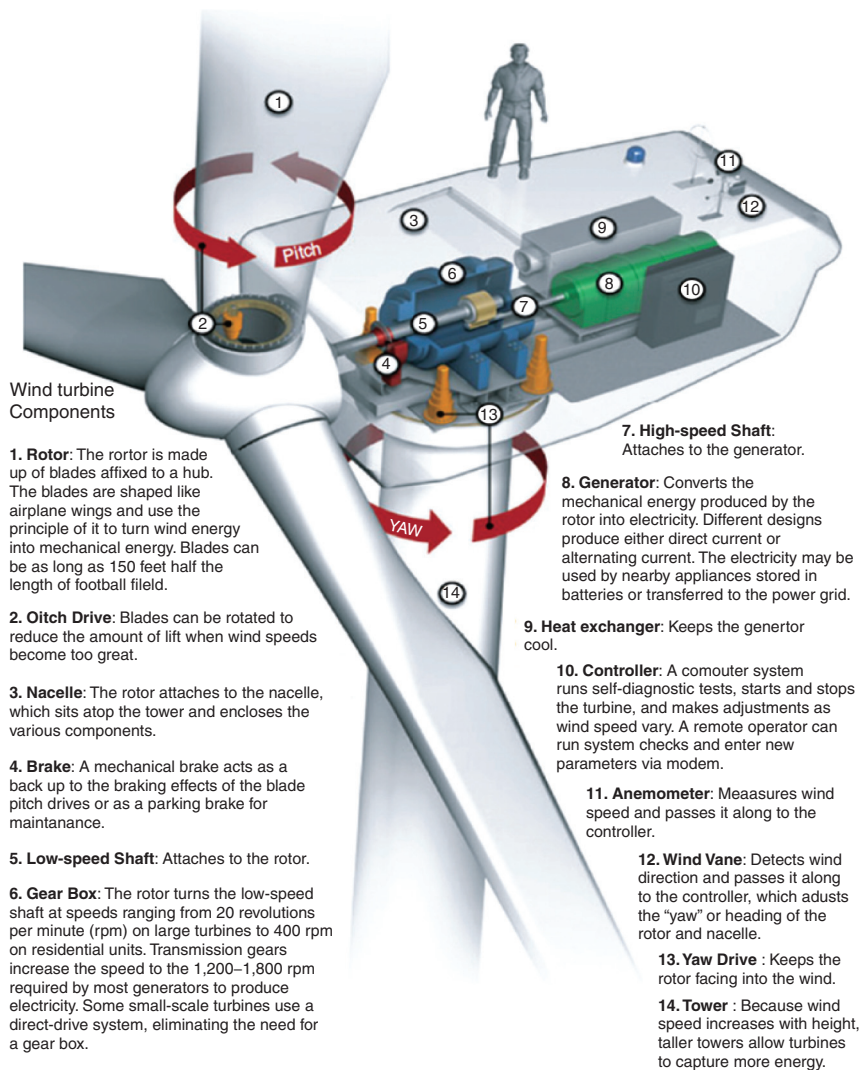
Figure 5 Siemens HAWT (model: SWT-2.3-82 VS) (http://www.energy.siemens.com/us/pool/hq/power-generation/wind-power/E50001-W310-A123-X-4A00_WS_SWT-2.3-82%20VS_US.pdf)

generally have much higher efficiency than VAWTs. The maximum power coefficient of a modern HAWT has been reported up to 45–50% while that of an efficient VAWT normally lies below 40% (Eriksson, Bernhoff, and Leijon 2008) (power coefficient of a Savonius-type VAWT is even lower, normally below 25% (Akwa, Vielmo, and Petry 2012)). Figure 5 shows a HAWT commercialized by SIEMENS (model: SWT-2.3-82 VS) (http://www.energy.siemens.com/us/pool/hq/power-generation/wind-power/E50001-W310-A123-X-4A00_WS_SWT-2.3-82%20VS_US.pdf).

As explained earlier, the rotor shaft of a HAWT is positioned in horizontal direction, i.e. parallel to the ground. The electric generator that is connected to the turbine rotor via the primary and secondary shafts is stored inside a nacelle box at the top of the tower. HAWTs are lift-type wind turbines and are very sensitive to changes in blade profile, design, and surface roughness. Another limitation with HAWTs is that they cannot catch the wind from all direction. They need a special mechanism to turn the rotor so that it always faces the wind. This was probably one of the main reasons why none of the historical HAWTs were so successful. In fact, the American windmill was the first HAWT which had a fully automatically controlled yaw system. Yaw system of a HWAT is basically a component which is responsible for the orientation of the wind turbine rotor toward the wind. In small size HAWTs, the yaw system comprises a simple roller bearing connected between the tower and the nacelle. A tail with a fin at the end is mounted on the back of nacelle which produces corrective moment to turn the wind turbine rotor into the wind. This type of yaw system is called "passive yaw system". The large-scale (MW) HAWTs however needs an active yaw mechanism. The active yaw systems are normally equipped with a wind sensor that senses the direction of wind and a servo motor that produces required torque to rotate the nacelle of the wind turbine against the stationary tower.

A HAWT, in general, consists of a rotor, a gear box, a generator, and a yaw system. The rotor of a HAWT includes two to three blades connected together with a hub. The hub is attached to a main shaft (sometimes also called primary shaft or low-speed shaft), which passes through bearings and connects to a gear-train. The gear train amplifies the rotational speed and provides higher rpm to a secondary shaft (sometimes also called high-speed shaft). The secondary shaft drives a generator that produces electricity. The gear-box, the primary and secondary shafts, and the generator are contained inside a nacelle box. The nacelle box also contains a yaw system to orient the rotor and a heat exchanger to cool down the generator. Figure 6 demonstrates all the major components of a large-scale modern HAWT (Crossley and Schubel 2012).

Wind turbine
Components

1. Rotor: The rortor is made up of blades affixed to a hub. The blades are shaped like airplane wings and use the principle of it to turn wind energy into mechanical energy. Blades can be as long as 150 feet half the length of football fileld.

2. Oitch Drive: Blades can be rotated to reduce the amount of lift when wind speeds become too great.

3. Nacelle: The rotor attaches to the nacelle, which sits atop the tower and encloses the various components.

4. Brake: A mechanical brake acts as a back up to the braking effects of the blade pitch drives or as a parking brake for maintanance.

5. Low-speed Shaft: Attaches to the rotor.

6. Gear Box: The rotor turns the low-speed shaft at speeds ranging from 20 revolutions per minute (rpm) on large turbines to 400 rpm on residential units. Transmission gears increase the speed to the 1,200–1,800 rpm required by most generators to produce electricity. Some small-scale turbines use a direct-drive system, eliminating the need for a gear box.

7. High-speed Shaft: Attaches to the generator.

8. Generator: Converts the mechanical energy produced by the rotor into electricity. Different designs produce either direct current or alternating current. The electricity may be used by nearby appliances stored in batteries or transferred to the power grid.

9. Heat exchanger: Keeps the genertor cool.

10. Controller: A comouter system runs self-diagnostic tests, starts and stops the turbine, and makes adjustments as wind speed vary. A remote operator can run system checks and enter new parameters via modem.

11. Anemometer: Meaasures wind speed and passes it along to the controller.

12. Wind Vane: Detects wind direction and passes it along to the controller, which adusts the "yaw" or heading of the rotor and nacelle.

13. Yaw Drive : Keeps the rotor facing into the wind.

14. Tower : Because wind speed increases with height, taller towers allow turbines to capture more energy.

Figure 6 Typical configuration of a modern large-scale HAWT (Crossley and Schubel 2012)

Large-scale vs small-scale wind turbines

The definition of "small"- and "large"-scale windmill has remained vague in the literature of wind energy. Small wind turbine was initially defined on the basis of its capability to produce electrical power sufficient enough to cover individual household electricity demands (Zhang 2012). But the problem lies in the fact that the consumption of electricity by a household itself is very debatable, because it varies with time and place. For example, an average American family needs a 10 kW turbine to cover their full consumption, while a European household requires a 4 kW turbine, which further reduces to a 1 kW turbine for an average Chinese household (Zhang 2012). Lacking any credible unanimous definition, the range for the rated power capacity of small-scale wind turbines (SSWTs) vary from few watts to few hundred kilowatts. Kishore, Coudron, and Priya (2013) have defined the nomenclature of HAWTs based on the size of the wind turbine rotor as given below. We will use the same nomenclature in this paper.

(i) Micro-scale wind turbine (μSWT): rotor diameter ≤ 10 cm,
(ii) Small-scale wind turbine (SSWT): 10 cm < rotor diameter ≤ 100 cm,
(iii) Mid-scale wind turbine (MSWT): 1 m < rotor diameter ≤ 5 m, and
(iv) Large-scale wind turbine (LSWT): rotor diameter > 5 m.

Need and applications of SSWTs

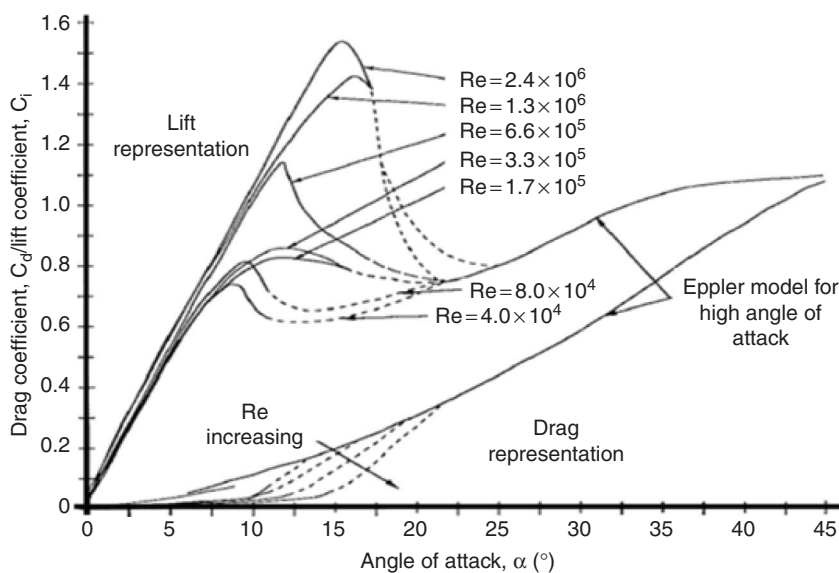The advancements achieved in the field of power electronics in the last few decades have vastly expanded the

deployment of wireless electronics. Not only the electronics have become smaller in size but also their power requirements have reduced by orders of magnitude. Currently, in majority of applications, lithium cell batteries are used, which limits the operation time and presents maintenance challenges because these batteries need to be regularly monitored and replaced. While the need of the batteries is growing exponentially over time, growth in battery capacity is proceeding along a flattening S-curve (Paradiso and Starner 2005). An alternative to batteries might be energy harvesting devices that can trap locally available environmental energy that mainly includes solar, wind, tidal, magnetic field, and vibrations. Out of these possibilities, the most reliable resource in terms of both availability and power density is the wind. However, the main concern is that the conventional LSWTs have very high operating wind speed, normally around 15 m/s, and thus they are installed several feet above the ground level. One of the key requirements for a wind turbine deployed for the purposes of charging the wireless microelectronics is its reliability while operating near the ground where wind is very weak due to boundary layer effect and obstacles like trees, buildings, and so forth. Unfortunately, most of the currently available SSWTs that operate at low wind speeds have poor aerodynamic performance which makes them economically unviable. The aerodynamic performance of a wind turbine is primarily influenced by Reynolds number of the airfoil used for the turbine blades. Reynolds number of an airfoil is given by:

$$Re = \frac{\rho c u_{rel}}{\mu} \qquad [1]$$

where ρ and μ are density and dynamic viscosity of the flowing fluid, respectively, c denotes the chord length of the airfoil, and u_{rel} is the relative wind speed. The Reynolds number of a wind turbine is proportional to the chord length and the wind speed. For the SSWTs, these two factors have very small value and therefore they operate at much lower Reynolds number as compared to the LSWTs. Figure 7 depicts the effect of Reynolds number on the aerodynamic parameters (lift and drag coefficients) for NACA 0012 airfoil (Kishore, Coudron, and Priya 2013; Musial and Cromack 1988). It is very interesting to note that the maximum lift coefficient decreases with decrease in Reynolds number while the drag coefficient increases when Reynolds number is reduced. This implies that the lift to drag ratio reduces sharply with decrease in Reynolds number, which results in poor performance of the SSWTs.

Literature review

There are very few papers available in literature that study the performance characteristics of SSWTs. Vardar and Alibas (2008) compared the rotation rates and power coefficients of various 31 cm diameter wind turbine rotor models. They were manufactured using four different NACA profiles (NACA 0012, NACA 4412, NACA 4415, and

Figure 7 Influence of Reynolds number on airfoil behavior (NACA 0012) (Kishore, Coudron, and Priya 2013; Musial and Cromack 1988)

NACA 23012). Various geometric parameters such as blade angle, twist angle, and blade number of these turbine models were investigated at different wind speeds. It was observed that the rotor with NACA 4412 profiles having 0° twist angle, 5° blade angle, and two blades had the highest rotation rate while the one with NACA 4415 profiles with 0° twist angle, 18° blade angle, and four blades had the highest power coefficient. A numerical study using blade element momentum theory and lifting line based wake theory was conducted by Duquette and Visser (2003) to assess the effects of blade number and solidity on the performance of 2 m diameter wind turbine. The study suggested that by increasing the solidity from the conventional range of 5–7% to 15–25% one can achieve better power coefficient values. Leung et al. (2010) optimized different blade parameters of a 23.4 cm diameter wind turbine using Computational Fluid Dynamics. The wind turbine used in this study had fan-type, mono-thick (constant thickness along the radius), and multiple numbers of blades instead of conventional airfoil type tapered blades. This study supported the fact that the higher solidity gives better performance to SSWTs, however it was also suggested that the blades should not fully occupy the swept area of the rotor to avoid blockage. It can be observed that all of these studies primarily focus on designing and optimizing the wind turbine rotor, more specifically the turbine blades. They lack the overall comprehensiveness addressing all the components together to develop a complete SSWT. Probably, the first attempt to make a complete SSWT was performed by Hirahara et al. (2005). They developed a four-bladed 50 cm diameter small wind turbine called μF500 using NACA 2404 airfoil. This turbine exhibited very good performance with power coefficient of 0.36 and overall efficiency of 0.25 in the wind speed range of 8–12 m/s.

Objectives of the paper

In this paper, we demonstrate small-scale wind energy portable turbine (SWEPT) targeted to operate near the ground level with high efficiency. SWEPT is a HAWT of rotor diameter about 40 cm, and it has been designed to operate at wind speeds below 5 m/s. Kishore, Coudron, and Priya (2013) and Kishore and Priya (2013) provide detailed description about the design specifications, fabrication processes, experimental testing, and power characteristics of two different generation prototypes of SWEPT. Table 2 summarizes the significant similarities and differences between the first and second generation

Table 2 Comparison between the first and second generation prototypes of SWEPT (Kishore, Coudron, and Priya 2013; Kishore and Priya 2013)

	First generation prototype	Second generation prototype
Axis of rotation	Horizontal	Horizontal
Rotor diameter	39.4 cm	40 cm
Number of blades	3	3
Tip radius	19.7 cm	20 cm
Hub radius	1.3 cm	3 cm
Twist angle	32°	37°
Blade type	Tapered	Constant chord
Chord length near root	5.7 cm	7.5 cm
Chord length near tip	2 cm	7.5 cm
Drive	Gear train with ratio 80:10	Gear train with ratio 80:10
Generator	24 V PM DC motor	24 V PM DC motor
Cut-in wind speed	2.7 m/s	3.0 m/s
Cut-out wind speed	5.0 m/s	5.5 m/s
Power coefficient	14%	32%
Optimal tip speed ratio	2.9	4.1
Maximum electrical power	0.83 W at 5 m/s	2.2 W at 5.5 m/s
Maximum overall efficiency	9%	21%

SWEPTs. It is very interesting to note that even though both the prototypes are of about the same size, the performance of the second generation prototype is much superior to that of the previous one. The prime reason behind this improvement is the difference between their blade designs. There are mainly six blade parameters that influence the aerodynamic performance of a wind turbine: airfoil, number of blades, twist angle, chord length, solidity, and tapering angle. The blades of the first prototype were of conventional design like most of the LSWTs, with linear twist and tapering from root to tip. On the other hand, the second generation SWEPT has blades specifically developed for the SSWTs at low wind speed applications. Its blade profile contains NACA 0012 airfoil, which is suitable for applications at the low Reynolds number. The blades were non-linearly twisted by 37° with higher twist near the hub that creates higher torque coefficient at low wind speed. The blades were not tapered like those of a conventional wind turbine rather they maintained constant chord length of 7.5 cm throughout their span.

In spite of the fact that the second generation SWEPT prototype had excellent efficiency of 21%, it is not a direct-drive wind turbine. Like the first generation prototype, it utilizes a gear train of gear ratio 80:10 to amplify the angular speed so that its generator can run at its rated rpm. The use of gear train however has several

limitations: (i) it increases the mechanical losses and thus reduces the overall efficiency of the device, (ii) the static friction between the gears increases the start-up wind speed of the wind turbine, (iii) running gears produce excess noise which is annoying, especially at high wind speed, (iv) at high wind speed, when gears run at very high rpm, they skid and thus limit the cut-out wind speed of the wind turbine, and (v) the wear and tear in the gears reduces the overall reliability and life span of the device. These problems can be avoided, if the wind turbine is direct drive. But, then the concern is the unavailability of a small size generator with required attributes (high efficiency, low rated angular speed of around 1,000 rpm, low starting torque of the order of few mN m, and high voltage to rpm ratio).

This paper also addresses the design and characterization of an axial flux generator developed to operate SWEPT without any gear drive. Wind tunnel experiments revealed that the axial flux generator allows the wind turbine to start at wind speed as low as 1.7 m/s. The wind turbine generates its rated electrical power of 1 W at 4.0 m/s wind speed. In comparison to previous prototypes that operate in a very narrow wind speed range of about 2.5–5.0 m/s (Kishore, Coudron, and Priya 2013; Kishore and Priya 2013), the current prototype operates in a much wider operating wind speed range of 1.7–10 m/s. The wind turbine was found to produce electrical power up to 9.8 W at the maximum tested wind speed of 10 m/s.

Generator design

There are several kinds of generators that are used for wind turbines: direct or alternating current types, synchronous or asynchronous, with or without permanent magnets (PM), and self or external electrical field excited machines. It has been suggested that the generators equipped with PMs are more suitable for small size wind turbines because of their higher efficiency compared with other generators (Ani, Polinder, and Ferreira). The PM electric generators are broadly divided into two categories: radial flux and axial flux machines, depending on the direction of magnetic flux in the air gap between stator and rotor. The radial flux generators can be further subdivided into inner rotor radial flux machines and outer rotor radial flux machines, according to the position of rotor with respect to stator. Similarly, axial flux generators can be subcategorized into double stator-single rotor machines and double rotor-single stator machines, based upon the number of rotors and

stators. Normally for SSWTs, an axial flux generator is preferred because it occupies lesser space in the radial direction than a radial flux generator of the same power rating (Ani, Polinder, and Ferreira; Park et al. 2012; Latoufis et al. 2012). A recent study by Marin et al. (under review) revealed that double rotor-single stator slotless axial flux generator design provides very promising results for µSWTs. The slotless axial flux generator design has several other advantages over other types of generators: (i) the topology of an axial flux machine leads to a short radial length which makes it very compact generator suited for small wind turbines; (ii) due to the slotless air-gap winding, the values of mutual and leakage inductances are low; and (iii) the absence of the slots provides noiseless operation with no cogging torque. In this study, therefore, we focused on the design and fabrication of a double rotor-single stator slotless axial flux generator.

As shown in Figure 8, a double rotor-single stator axial flux generator consists of a stator containing a set of coils and two rotors on either sides of the stator. Each of the rotors contains a set of PMs. Holding the coils stationary has both functional and operational advantages. It not only reduces the number of moving parts and thus renders a commutator unnecessary but also decreases the heating losses in the commutator and thus improves the efficiency. The proposed generator design has a slotless stator, and the coils are wound around the individual coil holders, unlike a typical DC generator where core of the machine consists of metallic slots and teeth around which the coils are wound. This design eliminates cogging torque and thus improves the start-up speed of the wind turbine. Cogging torque is the friction caused by the attraction between PMs and iron core present in a typical DC motor/generator, which increases the start-up torque and decreases the electrical efficiency at low wind speed.

Figure 8 A CAD model of the "double rotor-single stator slotless axial flux generator" without fixtures

Once the configuration of the generator was selected, the next step was to determine and optimize the various design parameters which are needed to achieve high efficiency under the given size constraints. Some of the main parameters which affect the performance of an axial flux generator are number of poles, air gap between stator and rotor, shape and size of magnets, and shape of the coils. The number of pole pairs is given by the following equation (Latoufis et al. 2012):

$$p = \frac{120 f_{\text{nom}}}{n_{\text{nom}}} \qquad [2]$$

Where p denotes number of pairs of magnetic poles, f_{nom} is the nominal armature EMF frequency, and n_{nom} represents the nominal angular speed of the rotor in rev/min (rpm). The rpm of rotor essentially depends on the wind speed; it increases as wind speed is increased. We selected the optimal angular speed of the wind turbine at its rated wind speed of 4.0 m/s, which is around 900 rpm, as the nominal rpm to calculate the number of pole pairs. Considering the applications of the SSWT, a DC voltage output is desired. Therefore, the AC output of the generator needs to be rectified, and thus no particular value of EMF frequency is mandatory. Higher number of magnet poles provide higher power-to-weight ratio of an electric generator, but it also increases the leakage of magnetic flux (Chalmers and Spooner 1999). We took the optimal number of magnetic poles equal to 8, which results in the EMF frequency of around 60 Hz at the rated wind speed of 4.0 m/s.

The procedure to obtain the optimized values of other three parameters, air gap between stator and rotor, shape and size of magnets, and shape of the coils is described below. To determine the optimum air gap, the electromagnetic induction model was utilized that has been described by Marin et al. (under review). The transformation factor $\Phi(t)$ which governs the rotational energy to electrical energy conversion is determined through the relationship:

$$U(t) = -\int \left(\vec{v} \times \vec{B} \right) \cdot \vec{dl} \cong -\dot{\theta} r \Phi(t) \qquad [3]$$

where $\vec{v}$ is the tangential coil velocity, $\vec{B}$ is the magnetic flux density cutting the coil, l is the conductor length, U_e is the EMF or instantaneous voltage generated, and $\dot{\theta}$ is the rotor angular velocity. By assuming that the coil velocity is orthogonal to magnetic field vectors, the line integral in eq. [3] reduces to eq. [4]:

$$U(t) = -\dot{\theta} r \int_{0}^{L_{\text{coil}}} B(t,r,\theta,z) \frac{r(r,\theta,z)}{r} dl \cos(\varphi(r,\theta,z)) \qquad [4]$$

where φ is the angle between $\vec{v} \times \vec{B}$ and the differential conductor length $\vec{dl}$, (r,θ,z) are coordinates within the coil volume, $r(r,\theta,z)$ is the distance from the center of rotation to the coordinate (r,θ,z), and r is the radius at edge of rotor. By discretizing the coil volume, eq. [4] is reduced to eq. [5] as:

$$\Phi(t) \cong \sum B(t,r,\theta,z) \Delta L_{\text{coil}} \left(\frac{r(r,\theta,z)}{r} \right) dl \cos(\varphi(r,\theta,z)) \qquad [5]$$

$$\Delta L_{\text{coil}} = \frac{L_{\text{coil}}}{\# \text{of volumes}} \qquad [6]$$

Using the above formulation, a transformation factor (Φ) was calculated. In order to calculate voltage and power using the transformation factor, Kirchoff's voltage law was applied in eqs [7] and [8].

$$0 = \Phi(t) r \dot{\theta} - (R_e + R_L) i(t) \qquad [7]$$

$$i(t) = \frac{\Phi(t) r}{R_e + R_L} \dot{\theta} \qquad [8]$$
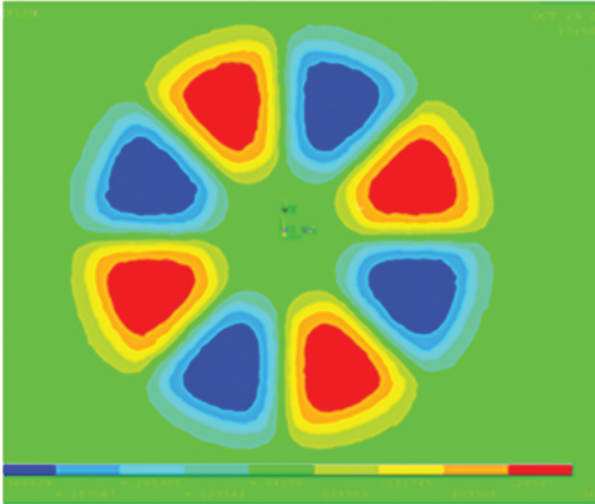
$$U_L(t) = i(t) R_L = \frac{\Phi(t) r}{R_e + R_L} \dot{\theta} R_L \qquad [9]$$

$$P_L(t) = i(t)^2 R_L = \frac{\Phi(t)^2 r^2}{(R_e + R_L)^2} \dot{\theta}^2 R_L \qquad [10]$$

With the assumption that $\Phi(t)$ has sinusoidal variation the average power can be calculated as:
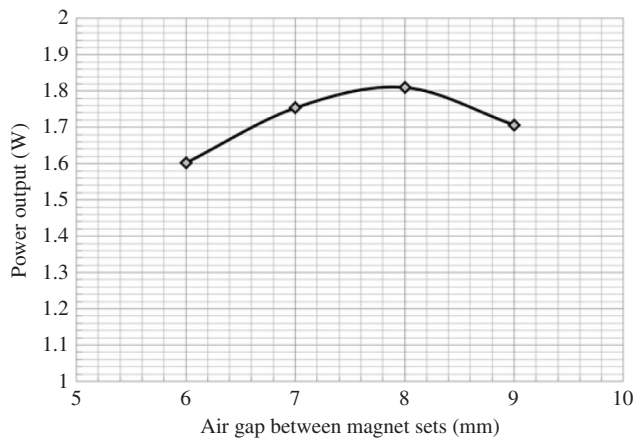
$$P_{\text{avg}} = \frac{\Phi_{\max}^2 r^2 \dot{\theta}^2}{2(R_e + R_L)^2} R_L \qquad [11]$$

We examined two different shapes of magnet: (i) rectangular and (ii) arc-shaped. It was numerically found that the arc-shaped magnets produce about 60% higher power than rectangular magnets of the same thickness and size. Considering the size of the generator (about the same diameter as the hub of the wind turbine), arc-shaped magnets of dimension 26.4 mm (or) × 10.5 mm (ir) × 6.35 mm (t) × 40° were selected, where, "or" and "ir" denote outer radius and inner radius, respectively, "t" denotes the thickness, and 40° is the angle made by inner and outer arc at the center. Figure 9 shows the contour for magnetic field strength at the mid-plane between two rotors. Dark red and dark blue indicate the highest field strength in two polarities. It can be noted that the magnetic field is in tear-drop shape, therefore, to

Figure 9 Contours showing the magnetic field strength at the mid-plane between two rotors

Table 3 Major design specifications of the axial flux generator developed for SWEPT

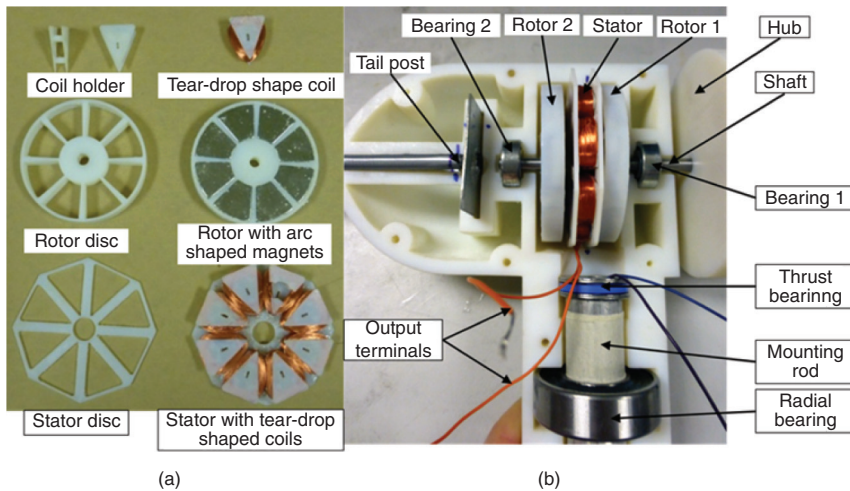|	
Number of pole pairs	8
Number of the magnets	16
Shape of magnets	Arc-shaped
Dimension of magnets	26.4 mm(or) $\times$ 10.5 mm(ir) $\times$ 6.35 mm(t) $\times$ 40°
Shape of coils	Tear drop
Number of coils	8
Number of turns per coil	150
Coil wire material	AWG 30 copper
Stator thickness	5 mm
Air gap between rotors	10 mm
Outer radius	3 cm
Inner radius	5 mm

match the profile of magnetic field, coils were also designed to have a tear-drop shape rather than the common circular shape. Lastly, the numerical simulations predicted that the maximum power output by the generator occurs when the air-gap between the rotors is about 8 mm (Figure 10). This distance was increased to 10 mm during fabrication due to the manufacturing constraints using human hands.

Figure 10 Effect of air gap on power output of the generator

Table 3 summarizes the major design specifications of the axial flux generator developed for SWEPT. Figure 11(a) depicts the fabricated stator and rotor parts, while Figure 11(b) demonstrates a fabricated prototype of the axial flux generator set along with other main components assembled inside the nacelle box.

Prototype design

Figure 12 shows the current generation prototype of SWEPT. It can be noted that SWEPT is three-bladed HAWT. It employs NACA 0012 airfoil template for the blade design. Each of the blades has constant chord length of 7.5 cm throughout the span. The hub and tip diameters of the wind turbine rotor are 3 cm and 40 cm, respectively. The blades are non-linearly twisted by 37 from hub to tip, and the solidity of the rotor is about 30%. As shown in Figure 11(b), SWEPT's nacelle box consists of an axial shaft, two bearings, a generator set, and a tail post. The nacelle is mounted over a tower using a thrust bearing and a radial bearing. The central shaft is 3/16 inch (4.76 mm) in diameter. The bearings used are high-load steel ball bearings, which are oil lubricated and unshielded from both the sides to minimize the frictional losses. The hub was connected with the central shaft using press-fit, while the blades are attached with the hub using dove-tail joints. The nacelle box also contains a tail with a fin at the end, which produces corrective moment to orient the wind turbine rotor into the direction of wind. The blades, hub, and nacelle box were constructed using a 3-D printer (Objet Inc., USA). The printer material used was VeroWhite plastic.

Experimental set-up

Figure 13 depicts the schematic of experimental set-up used in this study to characterize the wind turbine. All the experiments were conducted in Subsonic Open Jet Wind Tunnel facility available in Aerospace & Ocean

Figure 11 Axial flux generator design for SWEPT: (a) fabricated stator and rotor parts showing the shapes of the magnets and coils and (b) axial flux generator inside the nacelle box

Figure 12 An experimental prototype of "SWEPT"

Engineering department at Virginia Tech. The details about the wind tunnel and the quality of flow are given in Kishore, Coudron, and Priya (2013) and Kishore and Priya (2013). We used non-contact type optical digital Tachometer "DT-209X" (SHIMPO Instruments, USA) to measure the angular speed of the wind turbine. Anemometer used in the experiments was PASPORT, Model PS-2174 (PASCO, USA). "OhmSOURCE Model OS-260" by IET Labs, Inc. was used as the resistance box to vary the loading conditions of the wind turbine. The multi-meter used to measure the output voltage of the

wind turbine generator was purchased from RadioShack. It can be seen from Figure 13 that the resistance box and the multi-meter are connected in parallel with the generator of the wind turbine. The load resistance can be varied using the resistance box at any given wind speed, and the corresponding output voltage can be recorded. Since the voltage output of this generator was alternating, we measured the root mean square (rms) value to calculate the electrical power. We recorded continuous data for voltage and angular velocity at the given loading conditions and wind speeds, and then the arithmetic mean was calculated as the representative value for the respective variables. The experiments were carried out at various wind speeds between 1.5 m/s and 10 m/s.

Results and discussion

Generator characteristics

To investigate the performance of a generator in laboratory, normally it is coupled with a dynamometer motor and the wind turbine is emulated by varying the speed of the dynamometer motor. In this study, however, we attached the generator directly to the wind turbine rotor and its characteristics were studied using wind tunnel experiments. Figure 14 depicts the output voltage profiles of the generator at various loading conditions and at constant wind speed of 3.2 m/s. It can be noted that the waveforms are practically sinusoidal. Increase in the load
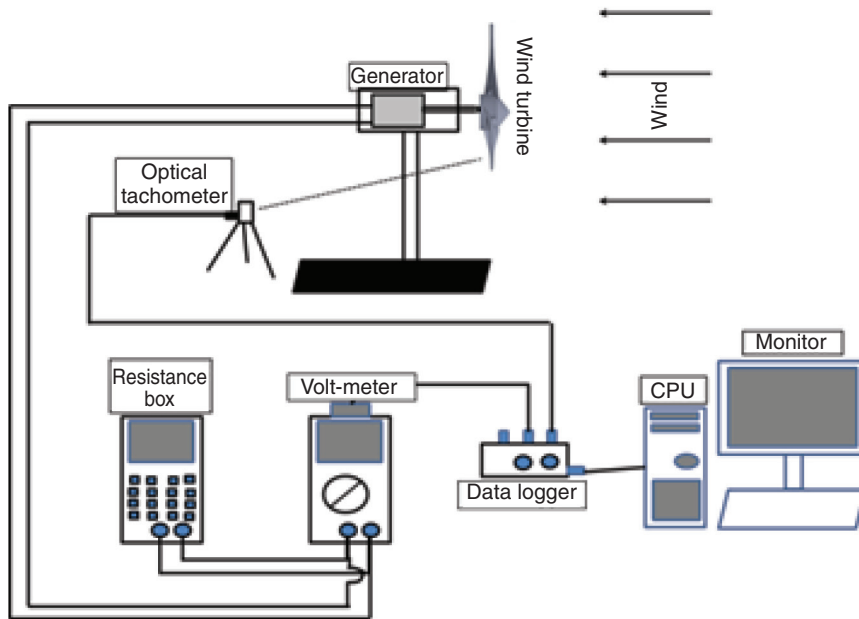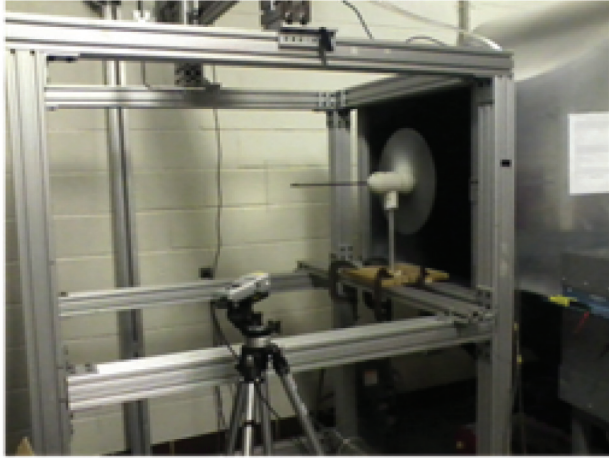
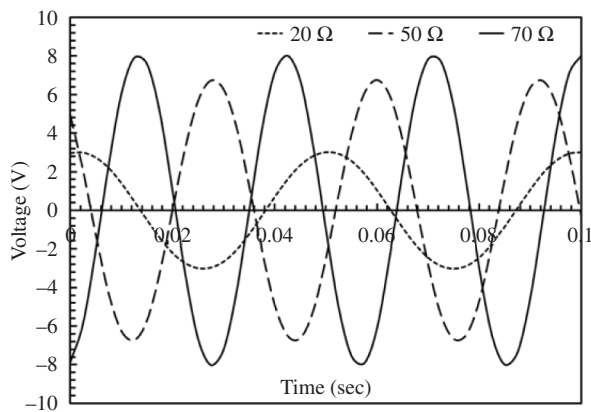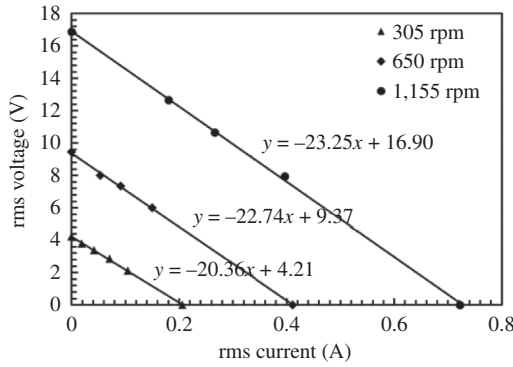**Figure 13** Schematic diagram of the experimental set-up

Figure 14 Output voltage profiles at various loading conditions (wind speed = 3.2 m/s)

resistance increases both the amplitude and the frequency of the voltage signal.

The internal impedance of the generator was measured by varying the load resistance and the wind speed in such a manner that the constant rotational speed of the wind turbine rotor is maintained. Figure 15 shows the variation of output rms voltage vs rms current at three different angular speeds. The slope of the curves gives the internal impedance of the generator at different frequencies (rpm). It should be noted that the value obtained is internal impedance, not internal resistance. The coil resistance of the generator was measured to be 19.6 Ω using a multi-meter. Looking at the slopes of the curves in Figure 10, it can be determined that the internal impedance is around 20.4Ω at 304 rpm (20.3 Hz), and it increases slowly with increase in the angular speed of the

Figure 15 Variation of generator voltage with current at different constant rpm conditions

Figure 17 Voltage vs angular speed at various loading conditions and wind speeds

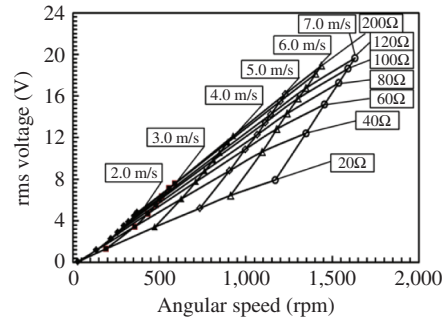rotor. The angular speed of the rotor is related to EMF frequency by following equation:

$$f = \frac{n^*p}{120} \quad [12]$$

where n denotes rpm of the rotor and p represents number of pole pairs. Increase in angular speed increases the EMF frequency which ultimately increases the reactance of the stator coils. However, it can be calculated that the reactance of the generator is very small in comparison to the resistance of the stator coils and therefore the generator's performance will be primarily influenced by internal resistance.

Figure 16 demonstrates the variation of root mean square (rms) voltage across the load as a function of load current under various loading conditions and the wind speeds. Voltage across the load is given by $V = IR$, where V is the voltage, I denotes the current, and R is the load resistance. It can be noted from Figure 16 that at a fixed value of load resistance, voltage increases almost linearly with increase in current. Also, as expected, slope of the lines increases with increase in load resistance.
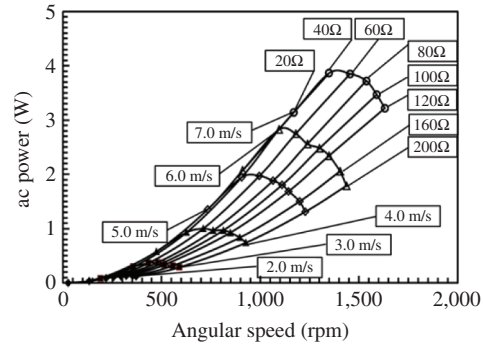
Increase in wind speed increases both the current and the voltage across the load, when load resistance is fixed. However, at the fixed value of wind speed, voltage and current has inverse relationship. Increase in load resistance increases the voltage but decreases the current.

Figure 17 shows the relationship between voltage and the angular speed at different load resistance and wind speeds. Theoretically, voltage by the generator is directly proportional to the angular speed of the shaft. As shown in Figure 17, for a fixed wind speed, voltage increases almost linearly with rpm. For a given value of wind speed, increase in load resistance causes increase in both, voltage by the generator and the angular speed of the rotor. Also, when external load is constant, increase in wind speed increases voltage as well as rpm. Figure 18 depicts the alternating power produced by the generator as a function of the angular speed of the shaft at various loading conditions and wind speeds. In can be noted that at a fixed load resistance, power by the generator increases with increase in shaft rpm. Also, for a given load, increase in wind speed increases the rotor speed as well as the power output because of the increase in aerodynamic torque on the rotor blades. For a fixed

Figure 16 Voltage vs current at various loading conditions and wind speeds

Figure 18 Power vs angular speed at various loading conditions and wind speeds

value of wind speed, the angular speed of the rotor increases with increase in load resistance. However, there exists an optimal load where power is highest, when wind speed is fixed.

The variation in shaft speed vs load resistance at various wind speeds is shown in Figure 19. Increase in wind speed increases the aerodynamic torque on the wind turbine rotor and therefore, at a fixed load resistance, shaft speed increases with increase in wind speed. However, at a fixed wind speed, rpm first increases with increase in load resistance, but it starts to saturate when load is too large. This can be explained if we understand the interaction between the stator and the rotors of the generator when the generator is at different loading conditions. When the connection is open circuit, there is no current in the stator coil and therefore no induced magnetic field. But, when a finite amount of resistive load is applied, it delivers current which creates a magnetic field around the stator coils that reacts with the magnetic field of the rotors. The strength of the reacting magnetic force between stator and rotors depends on the current which is ultimately determined by the magnitude of the load resistance. Higher load resistance results in lower current and thus lowers magnetic reaction, which causes increase in shaft rpm.
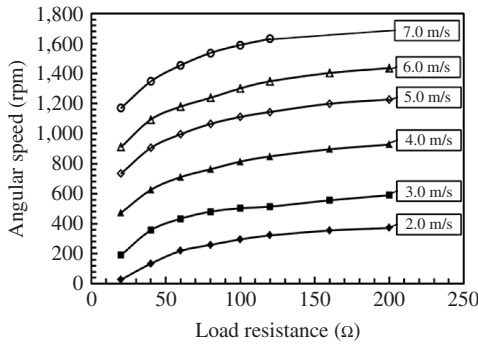

Figure 19   Angular speed vs load resistance at various wind speeds

Wind turbine performance

The direct-drive operation of the current generation SWEPT (with axial flux slotless generator) has two immediate advantages over the previous generation gear-drive prototypes: (i) the cut-in wind speed decreased to 1.7 m/s in comparison to 2.7 m/s of first generation prototype and 3.0 m/s of second generation prototype and (ii) the range of operating wind speed increased to 1.7–10 m/s in comparison to 2.7–5.0 m/s of first generation prototype and 3.0–5.5 m/s of second generation
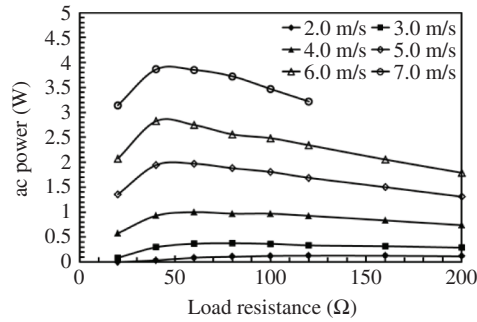

Figure 20   Power output vs load resistance at different wind speeds

prototype. Figure 20 shows the electrical power output of the wind turbine as a function of the load resistance at different wind speeds between 2.0 m/s and 7.0 m/s. At a fixed wind speed, the electrical power first increases with increase in load resistance, it reaches to a maximum value at an optimal load, and it decreases thereafter with further increase in the load resistance. Also, it can be seen that the electrical power increases with increase in wind speed because theoretically, power output of a wind turbine is proportional to cube of the wind speed. The optimal load decreases from 120 Ω at 2.0 m/s to 40 Ω at 7.0 m/s. The peak electrical power produced by the wind turbine is about 1 W at 4.0 m/s of wind speed, which increases to around 4 W at the wind speed of 7.0 m/s.

To investigate the performance of the wind turbine at higher wind speeds, we continued the wind tunnel experiment till 10 m/s. However, above 7.0 m/s of wind speed, the wind turbine was allowed to run only at its optimal load in order to obviate its operation at very high rpm. Figure 21 shows the variation of peak electrical power of the wind turbine as a function of wind speed. The experiment revealed that the wind turbine is capable of producing electrical power up to 9.8 W at the wind speed of 10 m/s. The net efficiency of the wind turbine is
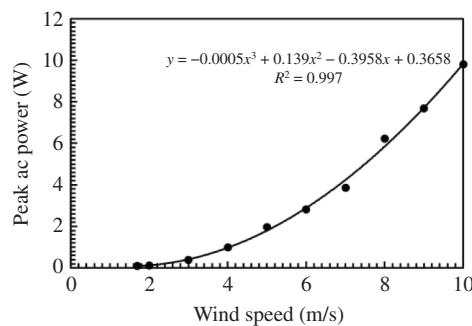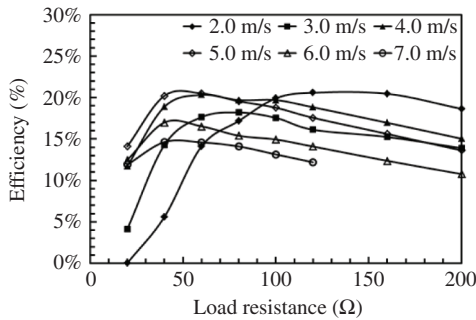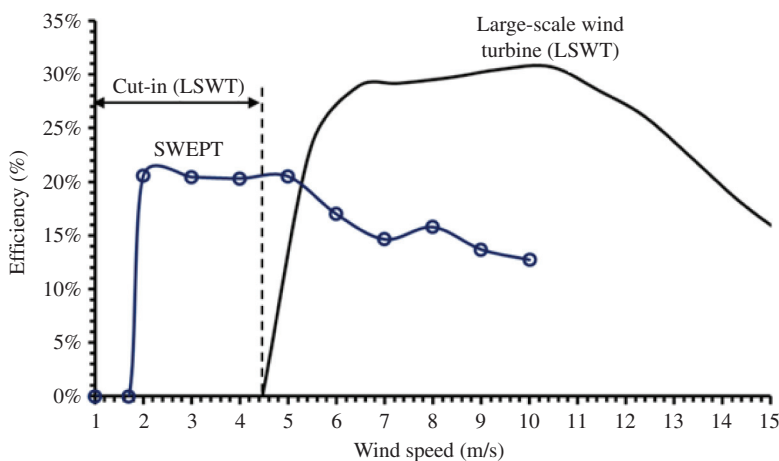

Figure 21   Peak electrical power vs wind speed

Figure 22   Net efficiency of the wind turbine vs load resistance at various wind speeds

shown in Figure 22. The wind turbine has maximum efficiency of about 21% at the rated wind speed of 4.0 m/s. It is also interesting to note that the peak efficiency of the wind turbine lies between 19% and 21% at lower wind speeds (2.0–5.0 m/s), however it decreases with further increase in the wind speed. This happens because the blades of the wind turbine have been specifically designed for low wind speed operations (rated wind speed of 4.0 m/s), which causes the wind turbine to stall when wind speed is increased above 5.0 m/s.

Lastly, Figure 23 demonstrates the peak efficiency of SWEPT vs that of a conventional large-scale megawatt wind turbine. LSWTs typically have overall efficiency of about 30–35%. However, there exists a cut-in wind speed of about 4.0–5.0 m/s where LSWTs do not operate. It is very interesting to note that in spite of the fact that SWEPT is a very small wind turbine and it operates within the cut-in wind speed region of the convention wind turbines, it still has about 60–70% efficiency in comparison to LSWTs.

Conclusions

In summary, this study presented the design, development, and experimental testing of an ultra-low start-up speed, highly efficient, direct-drive SWEPT. An axial flux generator was developed which is suitable for the small size wind turbines at low wind speed applications. Wind tunnel experiments were conducted to characterize the performance of the generator and the wind turbine. The major findings of the study can be summarized as follows:

(a) The cut-in speed of the wind turbine was found to be 1.7 m/s.
(b) The wind turbine operates in a very wide operating range of wind speeds, from few meters per second to 10 m/s.
(c) It produces electrical power of 1 W at its rated wind speed of 4.0 m/s.
(d) The peak power by the wind turbine increases to 4 W at 7.0 m/s, which further increases to 9.8 W at 10 m/s.
(e) The peak efficiency of the wind turbine was found to be around 21%. However, it decreases with increase in wind speed above 5.0 m/s.

Figure 23   Power efficiency curve of SWEPT vs a conventional LSWT

References

Akwa, J. V., H. A. Vielmo, and A. P. Petry. 2012. "A Review on the Performance of Savonius Wind Turbines." *Renewable and Sustainable Energy Reviews* 16(5):3054–64.

Ani, S. O., H. Polinder, and J. A. Ferreira. 2012. "Low Cost Axial Flux PM Generator for Small Wind Turbines." In: Energy Conversion Congress and Exposition (ECCE). IEEE, 2012.

Chalmers, B., and E. Spooner. 1999. "An Axial-Flux Permanent-Magnet Generator for a Gearless Wind Energy System." *IEEE Transactions on Energy Conversion* 14(2):251–57.

Crossley, R. J., and P. J. Schubel. 2012. "Wind Turbine Blade Design Review." *Wind Engineering* 36(4):365–88.

Duquette, M. M., and K. D. Visser. 2003. "Numerical Implications of Solidity and Blade Number on Rotor Performance of Horizontal-Axis Wind Turbines." *Journal of Solar Energy Engineering* 125(4):425.

Eriksson, S., H. Bernhoff, and M. Leijon. 2008. "Evaluation of Different Turbine Concepts for Wind Power." *Renewable and Sustainable Energy Reviews* 12(5):1419–34.

Gasch, R., and J. Twele. 2012. *Wind Power Plants – Fundamentals, Design, Construction and Operation*. Berlin, Heidelberg: Springer.

Global Wind Energy Council Report. 2012. "Global Wind Statistics."

Gsänger, S., and J. D. Pitteloud. 2012. *World Wind Energy Report 2011*. Germany: World Wind Energy Association (WWEA).

Hirahara, H., M. Z. Hossain, M. Kawahashi, and Y. Nonomura. 2005. "Testing Basic Performance of a Very Small Wind Turbine Designed for Multi-Purposes." *Renewable Energy* 30(8):1279–97.

Islam, M., D. S. K. Ting, and A. Fartaj. 2008. "Aerodynamic Models for Darrieus-Type Straight-Bladed Vertical Axis Wind Turbines." *Renewable and Sustainable Energy Reviews* 12(4):1087–109.

Kirke, B. K. 1998. *Evaluation of Self-Starting Vertical Axis Wind Turbines for Stand-Alone Applications*. Doctoral dissertation, Griffith University.

Kishore, R. A., T. Coudron, and S. Priya. 2013. "Small-Scale Wind Energy Portable Turbine (SWEPT)." *Journal of Wind Engineering and Industrial Aerodynamics* 116:21–31.

Kishore, R. A., and S. Priya. 2013. "Design and Experimental Verification of a High Efficiency Small Wind Energy Portable Turbine (SWEPT)." *Journal of Wind Engineering and Industrial Aerodynamics* 118:12–19.

Latoufis, K., G. Messinis, P. Kotsampopoulos, and N. Hatziargyriou. 2012. "Axial Flux Permanent Magnet Generator Design for Low Cost Manufacturing of Small Wind Turbines." *Wind Engineering* 36(4):411–32.

Leung, D. Y. C., D. Y. C. Leung, Y. Deng, and M. K. H. Leung. 2010. "Design Optimization of a Cost-Effective Micro Wind Turbine." *Lecture Notes in Engineering and Computer Science* 2184(1):988–93.

Marin, A., R. Kishore, D. A. Schaab, D. Vuckovic, and S. Priya. "Micro Wind Turbine for Powering Wireless Sensor Nodes." *Energy Harvesting and Systems* (under review).

Musial, W. D., and D. E. Cromack. 1988. "Influence of Reynolds Number on Performance Modeling of Horizontal Axis Wind Rotors." *Journal of Solar Energy Engineering* 110(2):139–44.

Paradiso, J. A., and T. Starner. 2005. "Energy Scavenging for Mobile and Wireless Electronics." *IEEE Pervasive Computing* 4(1):18–27.

Park, Y.-S., S.-M. Jang, J.-H. Choi, J.-Y. Choi, and D.-J. You. 2012. "Characteristic Analysis on Axial Flux Permanent Magnet Synchronous Generator Considering Wind Turbine Characteristics According To Wind Speed for Small-Scale Power Application." *IEEE Transactions on Magnetics* 48(11):2937–40.

Vardar, A., and I. Alibas. 2008. "Research on Wind Turbine Rotor Models Using NACA Profiles." *Renewable Energy* 33(7):1721–32.

WIND AND WATER POWER PROGRAM. 2011. "U.S. Department of Energy: Energy Efficiency and Renewable Energy."

Zhang, P. 2012. *Small Wind World Report 2012*. Germany: World Wind Energy Association (WWEA).